AIMS Materials Science, 13(5): 897–912.
DOI: 10.3934/matersci.2026042
Received: 06 July 2026
Revised: 17 September 2026
Accepted: 22 September 2026
Published: 10 October 2026

https://www.aimspress.com/journal/Materials

Research article

The excitation energy spectrum of the electron and spin subsystems of ferroelectrics and multiferroics, determined from ferroelectric and magnetic phase transitions

Danil V. Kuzenko* and Aleksey V. Bezus

Department of General and Theoretical Physics, Donetsk State University, 283001, Universitetskaya St., 24, Donetsk, Russian Federation

* **Correspondence:** Email: danil.kuzenko.84@yandex.ru; Tel: +7-949-605-0243.

Abstract: Ferroelectric materials and multiferroics are two classes of functional materials that exhibit unique electrical and magnetic properties that can be altered by external fields. Ferroelectrics are actively used as sensors, actuators, and energy storage devices, while multiferroics hold promise for future use in new types of memory and spintronic devices. Investigating the thermal excitation of the electron and spin subsystems of these materials is of theoretical and practical interest. Based on this, in this study, the vicinity of phase transitions exhibiting significant spin-phonon and electron-phonon interactions was analyzed for the ferroelectric $BaTiO_3$ and the multiferroics $YMnO_3$ and $HoMnO_3$: a second-order transition from the antiferromagnetic state to the paramagnetic state at the temperature for $YMnO_3$ and $HoMnO_3$; a first-order magnetostructural spin-reorientation transition for $HoMnO_3$; and a first-order ferroelectric phase transition of the displacement type at the Curie temperature for $BaTiO_3$. From the temperature dependences of the permittivity, magnetic permeability, and heat capacity, the activation energies of these quantities in the neighborhood of the phase transitions were obtained. It is suggested that the obtained activation energy values for magnetic and dielectric permeability can serve as parameters for estimating the excitation processes of the spin and electronic subsystems, respectively; this constitutes the novelty of this study.

Keywords: ferroelectric; multiferroic; phase transition; activation energy; permittivity; magnetic permeability; heat capacity; Curie temperature; Néel temperature; spin-reorientation transition

1. Introduction

The study of ferroelectric and magnetic phase transitions stands as a cornerstone of condensed matter physics, not only advancing our fundamental understanding of how ordered states emerge and evolve in materials but also underpinning the design and application of functional materials across a vast array of modern technical devices. Multiferroic materials that exhibit ferroelectric and magnetic order are of great research interest. Among these, perovskite-structured oxides with the general formula ABO_3 have emerged as the most intensively studied and widely utilized system. A key paradox in these materials lies in the "d^0 rule": this principle originally posits that ferroelectric order requires B-site cations to have a full d^0 electron configuration, which would inherently prohibit the coexistence of magnetism (which relies on partially filled *d*-orbitals). However, this contradiction is resolved for B-site cations with d^5–d^7 electron configurations, where a robust magnetoelectric coupling can arise through the multiferroic crossover effect. This phenomenon was first validated for $BiCoO_3$ via theoretical calculations that quantified the significant *p*–*d* hybridization between oxygen *p*-orbitals and cobalt *d*-orbitals [1]. For the broader "d^0–d^{10}" conundrum (i.e., enabling ferroelectricity in systems where B-site cations deviate from the d^0 configuration, including fully filled d^{10} states), two effective strategies have been established: (1) incorporating the pseudo-Jahn-Teller effect, which distorts the crystal lattice by lifting electronic degeneracy and driving spontaneous polarization; and (2) engineering geometric improper and hybrid improper ferroelectrics, where ferroelectric order emerges not from the displacement of individual ions (as in conventional proper ferroelectrics) but from the cooperative coupling and interaction of multiple phonon modes [2,3]. Alternatively, this can also be achieved by modulating the Mn–O–Mn bond angles, a process that is closely associated with the t_{2g} and e_g electron states in orthorhombic $TbMnO_3$ and $HoMnO_3$ [4]. Additionally, integrating theoretical and experimental research is of great significance. A representative example is the study on hexagonal manganite $YMnO_3$, which combined *X*-ray diffraction, structural analysis, and density functional theory calculations [5]. In the antiferromagnetic Mott perovskite insulator $Sr_{1-x}Ba_xMnO_3$, researchers used pulse-resolved inelastic *X*-ray scattering and far-infrared spectroscopy to identify a ferroelectric phase transition driven by the displacement of magnetic Mn^{4+} ions [6]. For $BiFeO_3$, inelastic neutron scattering measurements of the temperature-dependent phonon density of states and magnetic excitation spectra revealed pronounced anharmonicity, underscoring the critical role of spin-phonon coupling [7]. As demonstrated in $Eu_xBa_{1-x}TiO_3$, where Ba^{2+} ions are substituted with Eu^{2+}, targeted control of phonon anharmonicity enables a reduction in the temperature of the ferroelectric phase transition [8]. For magnetic phase transition, the spin-fluctuation theory and density of states model represent key theoretical frameworks [9]. Magnetic phase transitions are also a focus of study in artificial ferromagnetic materials: in layered Fe/MgO/Cr/MgO/Fe nanostructures, *X*-ray absorption spectroscopy has been employed to investigate the correlation between spin-orbit interaction and magnetic properties [10,11].

When describing ferroelectrics, one can use the terms "ferrons" (elementary excitations of electric dipole order, transferring polarization, momentum and energy in ferroelectrics) and "magnons" (elementary excitations of magnetic order, transferring spin, momentum and energy in magnets) [12–14]. This is not to be confused with "ferrons", magnetic polarons in antiferromagnets [15].

Electron paramagnetic resonance (EPR) and neutron magnetic resonance (NMR) methods also enable us to study the features of the phase transition. For example, for $Pb_5Ge_3O_{11}$ near the structural transition, a mechanism for broadening the EPR spectrum has been proposed that takes into account

the local fields of distant charge-compensating defects [16]. The development of the theory of the EPR and NMR line shape in disordered ferroelectrics is important [17].

Studies of the thermophysical properties of multiferroics are important for understanding the processes occurring during phase transitions. For $Bi_{1-x}Tm_xFeO_3$, the temperature dependence of the mean free path of phonons was determined in the region of the ferroelectric and antiferromagnetic phase transitions [18]. In mechanically activated nanostructured ceramics $SmFeO_3$, the excess heat capacity is due to: the multiplet structure of 4*f* electrons of Sm ions, dislocations, thermal generation of point defects, energy levels associated with polar displacements of Fe and Sm ions, and with a change in the angle between the oxygen octahedra of FeO_6 [19]. Additionally, for $PbFe_{0.5}Nb_{0.5}O_3$, anomalies in the heat capacity and thermal diffusion were found in the region of the diffuse ferroelectric phase transition Curie temperature (T_C) ≈ 380 K, the Burns temperature (T_d) ≈ 670 K, and the intermediate temperature (T^*) ≈ 470 K [20]. Additionally, for the relaxor $PbNi_{1/3}Nb_{2/3}O_3$ solar cell, up to a temperature of 400 K, measurements of the heat capacity did not reveal structural phase transitions [21].

Another method for studying phase transition is ferromagnetic resonance, the study of the frequency dependence of the spectrum of which in $La_{0.7}Sr_{0.3}MnO_3$ films and $SrIrO_3/La_{0.7}Sr_{0.3}MnO_3$ and $Pt/La_{0.7}Sr_{0.3}MnO_3$ heterostructures showed the emergence of a spin current flowing through the boundary of the heterostructures [22].

The study of the Mössbauer effect in $PbZr_{0.72}Sn_{0.28}O_3$ during phase transition enabled us to register two types of quadrupole splittings associated with different environments of the Sn ion occupying the center of the SnO_6 octahedra and to determine the non-equivalence of the Fe^{3+} ions in Cu_2FeBO_5, which occupy four different positions [23,24]. Moreover, for $HoFe_{1-x}Mn_xO_3$, we established the dependence of the spin-reorientation transition temperature (T_{SR}) on the Fe concentration, which was explained by the influence of Mn ions on the magnitude of indirect exchange in the Fe subsystem [25].

An important method is *X*-ray photoelectron spectroscopy, which enables us to, for example, determine the ratio of manganese Mn^{3+}/Mn^{4+} in the ceramic composite $Bi_{1-x}La_xFe_{1-y}Mn_yO_{3+\sigma}$ [26]. The determination of the phase composition and the presence of phase transitions is carried out by *X*-ray diffraction and Raman spectroscopy, which was done for the $Ba_{0.7}Sr_{0.3}TiO_3$ multiferroic doped with Fe^{3+} and Co^{2+} [27].

It is also worth noting the computational methods in the physics of phase transitions. These include, for example, the application of the Monte Carlo method to study magnetic phase transitions in $(1-x)BiFeO_{3-x}PbFe_{1/2}Sb_{1/2}O_3$ [28]; calculation of the electronic and mechanical properties of $KNbO_3$ and $RbNbO_3$ using the density functional theory [29]; Hamiltonian modeling of the microscopic mechanisms of "incorrect" ferroelectric in multiferroic perovskites ($HoMnO_3$) [30]; and ab initio determination of the electronic band structure of $SrTiO_3$, $BaTiO_3$, and $CaTiO_3$ [31].

In complex transition metal oxides, oxygen vacancies are important. Thus, in $YMnO_3$, the peak in the temperature dependence of the permittivity at temperatures from 300 to 473 K is due to polaron jumps with an activation energy of 0.36 eV, and the peak at temperatures from 473 to 673 K is due to electron jumps caused to the second ionization of oxygen vacancies with an activation energy of 1.13 eV [32]. For $BaTiO_3$, the activation energy of oxygen vacancy motion is determined by the EPR method: 0.91 eV [33]. Moreover, in $KNbO_3$, the dielectric relaxation is explained by the relaxation of dipoles associated with oxygen vacancies, with an activation energy of 0.84 eV [34].

Higher values of the activation energy (2.07 eV) for a process close to the phase transition temperature are explained by the interaction of the defect and domain structures of the ferroelectric [35].

2. Materials and methods

Here, we used ceramic samples of $BaTiO_3$, synthesized at a temperature of 1670 K, obtained at the Scientific Research Institute "Reaktivelectron". The completeness of the synthesis and the production of single-phase $BaTiO_3$ were monitored by *X*-ray diffraction (DRON-3, Cu-Kα radiation). The phase transition study was conducted by measuring the temperature dependence of the heat capacity of the samples using a differential scanning calorimetry setup (ThermoScan-2, Analitpribor), as well as the temperature dependence of the permittivity using a broadband immittance analyzer (E7-28, MNIPI) at a frequency of 1 kHz in the temperature range from 300 to 500 K.

The results of the experimental data on hexagonal single crystals of $YMnO_3$ and $HoMnO_3$ were also analyzed [36]. Polycrystalline powders of these were synthesized using a solid-state reaction at a temperature of 1323 K and sintered at 1523 K. The growth of the single crystals was carried out in an optical floating zone furnace (Crystal System Incorporation). The crystal structures and physical properties were characterized using *X*-ray diffraction (XRF-1800, Shimadzu), magnetic susceptibility (SQUID-VSM, Quantum Design), specific heat capacity (PPMS, Quantum Design), resistivity, and permittivity measurements at 50 kHz along the c-axis (Agilent 4294A) [36].

Relative magnetic permeabilities were calculated from magnetic susceptibility measurements of $YMnO_3$ and $HoMnO_3$ single crystals in a 0.1 T magnetic field applied along the c-axis [36].

To obtain the activation energies of the electron and spin subsystems near the phase transition, the experimental results were analyzed using our proposed method.

3. Results and discussion

In a study of the temperature dependence of the permittivity of the $Pb(Zr,Ti)O_3$ ferroelectric, we previously established the presence of a critical temperature below the Curie temperature, at which the domain structure decomposes, which subsequently made it possible to determine the activation energies of defects in $Pb(Zr,Ti)O_3$ using the temperature activation-relaxation method of permittivity [37,38]. Based on this, in this work, we propose to continue the study of activation processes in the vicinity of ferroelectrics and magnetic phase transitions to determine the spectrum of activation energies of excitation processes of the electron and spin subsystems. For this purpose, the activation processes of the following phase transitions are considered:

- A second-order transition from the antiferromagnetic state to the paramagnetic state at the Néel temperature (T_N) ($YMnO_3$, $HoMnO_3$).
- A first-order magnetostructural transition of the order-to-order type at the T_{SR} ($HoMnO_3$).
- A first-order ferroelectric phase transition of the displacement type ($BaTiO_3$).

Hexagonal $YMnO_3$ and $HoMnO_3$ are multiferroic because they are ferroelectric below 900 and 830 K and antiferromagnetic below $T_N \approx 70$ K.

For $BaTiO_3$, the ferroelectric phase transition at temperature T_C is accompanied by structural changes in the crystal lattice symmetry from tetragonal to cubic. However, for $YMnO_3$ and $HoMnO_3$ at temperatures T_N and T_{SR}, the crystal lattice symmetry is hexagonal, and only the symmetry of the magnetic sublattice changes. This, as noted in [39], can be considered a magnetostructural phase

transition. Therefore, in what follows, it is appropriate to consider ferroelectric and magnetic phase transition within the framework of a unified activation approach.

The oxides $BaTiO_3$, $YMnO_3$, and $HoMnO_3$ studied in this work contain ions of transition (Ti, Mn) and rare-earth (Y, Ho) elements. As a result of complex interactions between the moments of the electrons of the 3*d* and 4*f* shells, $YMnO_3$ and $HoMnO_3$ exhibit interesting effects caused by the complex interaction of two magnetic subsystems [38]. In the case of $BaTiO_3$, polar instability associated with the occurrence of spontaneous polarization is caused by the hybridization of the 2*p* states of oxygen with the 3*d* states of the transition metals [40].

The approach to the analysis of the temperature dependences of the heat capacity ($C_p(T)$) in the vicinity of the phase transition, also used in [41], made it possible to determine the jump in the heat capacity (ΔC_p) caused by the phase transition for $YMnO_3$, $HoMnO_3$, and $BaTiO_3$ (Figure 1).

In particular, for $YMnO_3$ and $HoMnO_3$, the vicinity of the antiferromagnetic transition at the $T_N \approx 70$ K, associated with the ordering of the Mn^{3+} moments in a non-collinear arrangement (Figure 1a,b), was analyzed. For $BaTiO_3$, the vicinity of the ferroelectric phase transition of the displacement type was analyzed at the $T_C \approx 394$ K, associated with a change in the symmetry of the crystal lattice (Figure 1c).

In this paper, a critical temperature, denoted as $T_{crit.}$, is introduced; it corresponds to the onset of an activation process preceding the phase transition (T_C, T_N, or T_{SR}). For the ferroelectric phase transition at the T_C, the probability of transitions between the 3*d* levels of the transition metal and the 2*p* levels of oxygen increases at $T_{crit.}$. For the antiferromagnetic phase transition at the T_N and the spin-reorientation phase transition at T_{SR}, this temperature $T_{crit.}$ corresponds to the onset of irreversible rotation of the magnetization vector and a change in spin symmetry, respectively.

This approach is based on the additivity of the contributions of the heat capacities of the Debye model (C_D), of the heat capacities of the phonon anharmonicity ($C_{anh.}$) and of the heat capacities of the phase transition ($C_{p.t.}$) to the experimentally determined value of the heat capacity (C_p) according to the Eq 1:

$$C_p(T) = C_D(T) + C_{anh.}(T) + C_{p.t.}(T) \tag{1}$$

To find the ΔC_p caused by the phase transition, the experimental dependence $C_p(T)$ (Eq 1), with the exception of the region in the vicinity of the phase transition, is approximated by a polynomial according to the Eq 2:

$$C_p^{approx.}(T) = a \cdot T^3 + b \cdot T^2 + c \cdot T + d \tag{2}$$

where *a*, *b*, *c*, and *d* are coefficients, and *T* is the temperature, and $C_p^{approx.}(T)$ is the temperature dependence of the heat capacity in the vicinity of the phase transition, approximated by Eq 2. The jump in heat capacity is determined from Eq 3:

$$\Delta C_p(T) = C_p(T) - C_p^{approx.}(T) \tag{3}$$

In our model, the heat capacity of the phase transition (as well as the permittivity and magnetic permeability) is considered an activation process with the activation energy of the heat capacity (U_C), according to the exponential dependence according to the Eq 4:

$$\Delta C_p(T) = C_0 \cdot exp(-\frac{U_C}{k \cdot T}) \tag{4}$$

where C_0 is the coefficient, k is the Boltzmann constant, T is the temperature. The "–" sign corresponds to the activation process in the antiferromagnetic or ferroelectric phase. The analysis revealed the presence of $T_{crit.}$, which is lower than the T_C and the T_N ($T_{crit.} < T_C$, $T_{crit.} < T_N$), enabling us to determine the activation energy of heat capacity U_C in the temperature range from $T_{crit.}$ to T_C, in which the dependence $C_p(T)$ satisfies an exponential dependence according to Eq 4 (Figure 1, Table 1).

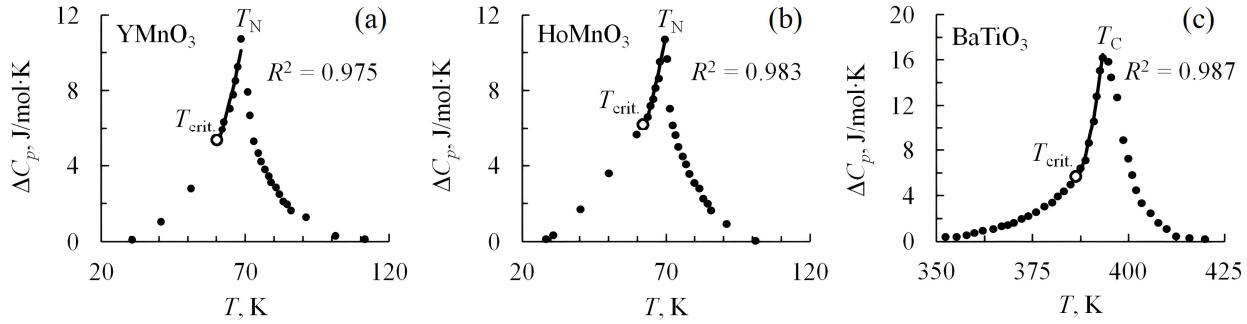


Figure 1. Temperature dependence of the heat capacity jump in the vicinity of the phase transition of (a) $YMnO_3$, (b) $HoMnO_3$ single crystals, and (c) $BaTiO_3$ ceramics. Points are experimental data using Eq 3. Lines are calculated using Eq 4.

The physical mechanisms of the identified activation processes are determined by the type of phase transition in the specified temperature range (Figure 1): bias-type ferroelectric for $BaTiO_3$ and antiferromagnetic for $HoMnO_3$ and $YMnO_3$, which, in turn, are caused by excitation of the electron and spin subsystems. This enables us to consider the study of phase transitions as a method for determining the temperature excitation spectrum of the electron and spin subsystems of ferroelectrics, magnets, and multiferroics.

Table 1. Calculated values of activation energy (U), critical indices of heat capacity (α) and susceptibility (γ) and the approximation reliability (R^2) values for $YMnO_3$, $HoMnO_3$, and $BaTiO_3$. AP is the activation parameter: μ is the magnetic permeability; ε is the dielectric permittivity.

Sample	AP	Phase transition	U, eV	R^2 (U)	α	R^2 (α)	γ	R^2 (γ)
$YMnO_3$	μ	$T_N \approx 70$ K	1.12×10^{-6}	0.980	-	-	1.15×10^{-5}	0.956
	ΔC_p	$T_N \approx 70$ K	2.98×10^{-2}	0.975	0.294	0.980	-	-
$HoMnO_3$	μ	$T_{SR} \approx 41$ K	1.53×10^{-5}	0.943	-	-	1.08×10^{-4}	0.896
	ε	$T_{SR} \approx 41$ K	2.77×10^{-3}	0.992	-	-	6.12×10^{-3}	0.996
	ΔC_p	$T_N \approx 70$ K	3.09×10^{-2}	0.983	0.257	0.980	-	-
$BaTiO_3$	ε	$T_C \approx 394$ K	2.28	0.972	-	-	6.38×10^{-1}	0.966
	ΔC_p	$T_C \approx 394$ K	2.29	0.987	0.445	0.964	-	-

Given the significant electron and spin-phonon interactions in ferroelectrics and magnets, an exponential dependence can also be used to analyze the temperature dependences of the magnetic permeability μ(T) and dielectric permittivity ε(T) in the vicinity of the phase transition, according to Eqs 5 and 6:

$$\mu(T) \sim exp(-\frac{U_\mu}{k \cdot T}) \tag{5}$$

$$\varepsilon(T) \sim exp(-\frac{U_\varepsilon}{k \cdot T}) \tag{6}$$

It is worth noting that the exponential law description of magnetic permeability and dielectric permittivity (Eqs 5 and 6) is valid only in the vicinity of the phase transition, where significant excitation of the electron and spin subsystems is observed. This is also possible for the heat capacity, which is largely determined by the phonon contribution, through electron-phonon and spin-phonon interactions. The hypothesis of a temperature-activation mechanism for the temperature dependence of permittivity was previously substantiated (using $Pb(Zr,Ti)O_3$ and $BaTiO_3$ as examples), and the possibility of describing it by an exponential dependence (in the vicinity of the phase transition) was demonstrated in [35].

The validity of applying the activation energy analysis method to heat capacity and susceptibility (magnetic and electric) near a phase transition deserves special attention. Generally, for magnets and dielectrics, the dependences of heat capacity and susceptibility on temperature and external fields can be related through common fundamental principles and critical phenomena. This relationship is manifested through the fluctuation-dissipation theorem: susceptibility is related to energy dissipation (energy loss due to overcoming resistances), while heat capacity is related to the density of states and the number of degrees of freedom. Near a second-order (or first-order phase transition close to second-order phase transition) phase transition (magnetic or ferroelectric), the scale of fluctuations increases sharply, leading to a consistent enhancement of both susceptibility (permeability) and heat capacity. This relationship is also manifested in the presence of standard power-law critical behavior.

It is known that measurements of the temperature dependences of thermodynamic variables, heat capacity C and susceptibility χ (magnetic and dielectric) near the points of second-order phase transitions (or first-order phase transitions close to second-order phase transitions), show that these quantities experience power-law singularities at the temperatures of the phase transition (T_{PT}).

An analysis of the experimental data for the materials we studied showed that the dependences $C(T)$, ε(T), and μ(T) in the temperature range from $T_{crit.}$ to T_{PT} ($T_{PT} = T_C$, T_{SR}, T_N) follow a power-law critical behavior (Table 1) in accordance with Eqs 7 and 8:

$$C \sim (T_{PT} - T)^{-\alpha} \tag{7}$$

$$\chi \sim (T_{PT} - T)^{-\gamma} \tag{8}$$

where α and γ are constants called critical indices and play a central role in the theory of critical phenomena. For ferroelectric and magnetic crystals, in most cases, Landau's theory for second-order phase transitions yields critical indices of α = 0 and γ = 1 up to the immediate vicinity of the phase transition point [42,43]. However, Landau's theory of second-order phase transitions is notorious for its failure to account for fluctuations in the displacement of ions from symmetric positions in the

so-called “critical region”, where the crystal’s properties are highly sensitive to external influences. In this “critical region”, Landau’s theory is no longer applicable, and the fluctuation theory of phase transitions takes over.

However, in practice, the values of critical indices often differ from the theoretical ones (α = 0 and γ = 1). This is true for the antiferromagnet Cr_2O_3 near the critical region. A crossover from Heisenberg critical behavior with n = 3 to Ising critical behavior with n = 1 (n is the number of degrees of freedom of the order parameter) was discovered, and it was determined that the value of the critical index α can take values from −0.1 to 0.1 [44].

We will show that the power-law dependencies (Eqs 7 and 8) can be reduced to Eqs 4–6, which enable us to determine the activation energy of the process preceding the phase transition. To do this, we equate the corresponding equations, for instance, for the heat capacity C, taking into account the proportionality coefficient a and the fact that the activation process begins at the $T_{crit.}$. Based on this, we obtain Eq 9:

$$a \cdot (T_{PT} - T_{crit.})^{-\alpha} = exp(-\frac{U_C}{kT_{crit.}}) \quad (9)$$

Using the Maclaurin series expansion of the exponential function and retaining only the first-degree term, from Eq 9 we obtain Eq 10:

$$U_C = (1 - \frac{a}{T_{PT} - T_{crit.}})\alpha k T_{crit.} \quad (10)$$

It is also worth briefly mentioning the statistical-mechanical basis for the exponential description of the $C(T)$, $\varepsilon(T)$, and $\mu(T)$ dependencies. Here, it can be noted that in the temperature range near the phase transition, where the system loses stability, fluctuations of the order parameter $\Delta\eta$ and the associated macroscopic quantities should increase significantly. In this case, the mean square of fluctuations in a certain region ΔV of the system is given by an Eq 11:

$$\overline{(\Delta\eta)^2} = \frac{\int_{-\infty}^{\infty}(\Delta\eta)^2 \, exp(-\frac{U}{kT}\Delta V)\, d(\Delta\eta)}{\int_{-\infty}^{\infty} exp(-\frac{U}{kT}\Delta V)\, d(\Delta\eta)} \quad (11)$$

which includes an exponential factor containing the activation energy [42]. The relationship of heat capacity and susceptibility to the order parameter described by Eq 11 makes it possible to use statistical mechanics to determine the $C(T)$, $\varepsilon(T)$, and $\mu(T)$ dependencies in the vicinity of the phase transition.

Figure 2a shows that in the studied regions of the temperature dependence of permittivity, an anomaly is observed at the temperature T_N for $YMnO_3$, and at the temperature T_{SR} for $HoMnO_3$.

Based on this, the analysis of experimental data on the temperature dependence of magnetic permeability $\mu(T)$ for $YMnO_3$ and $HoMnO_3$ using Eq 5 made it possible to determine the activation energies of magnetic permeability U_μ in the vicinity of the phase transition (Table 1).

For $YMnO_3$, the vicinity of the antiferromagnetic transition at the temperature $T_N \approx 70$ K was studied. This transition is caused by the ordering of Mn^{3+} moments into a non-collinear arrangement with magnetic symmetry P6′$_3$cm′ as a result of the competition of magnetic anisotropy in the sublattices of rare-earth and transition metals (Figure 2b). For $HoMnO_3$, the vicinity of the spin reorientation transition at temperature $T_{SR} \approx 41$ K was studied. This transition is caused by the

reorientation of the Mn^{3+} sublattice spin relative to the crystallographic axes with a change in magnetic symmetry from P6′$_3$c′m to P6′$_3$cm′ (Figure 2c).

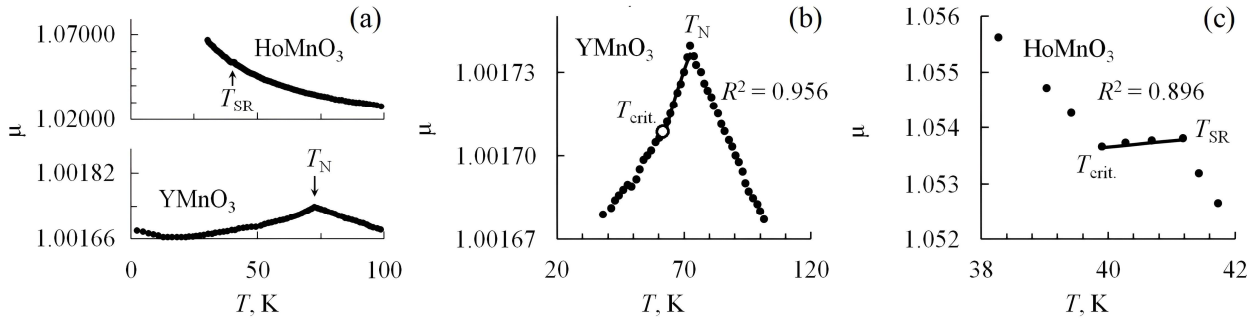


Figure 2. Temperature dependence of the magnetic permeability of (a) $YMnO_3$ and $HoMnO_3$ at low temperatures, as well as (b) $YMnO_3$ and (c) $HoMnO_3$ in the vicinity of the phase transition. Points are experimental data. Lines are calculated from Eq 5.

The temperature dependence of the permittivity of $YMnO_3$ and $HoMnO_3$ (Figure 3a) shows no anomalies at the temperature T_N, while at the T_{SR}, a jump in the dependence is observed only for $HoMnO_3$.

Based on this, an analysis of the experimental data on the temperature dependence of permittivity ε(T) for $HoMnO_3$ and $BaTiO_3$ using Eq 6 enabled us to determine the activation energies of permittivity U_ε in the vicinity of the phase transition (Table 1).

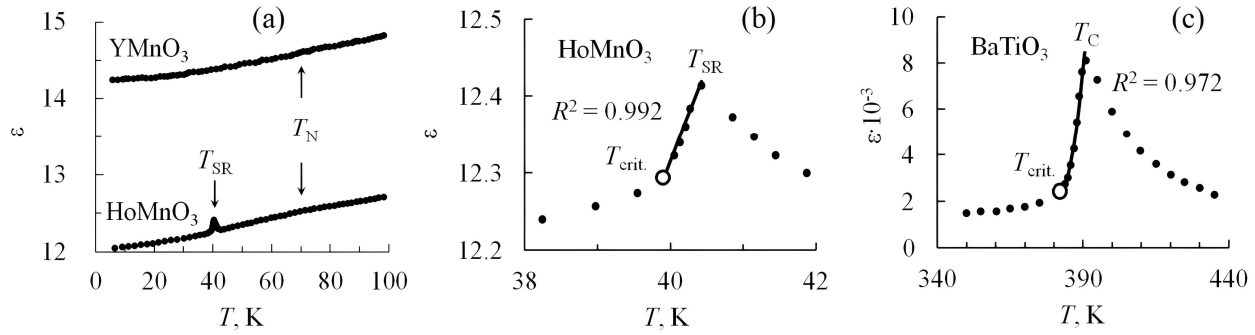


Figure 3. Temperature dependence of the permittivity of (a) $YMnO_3$ and $HoMnO_3$, as well as (b) $HoMnO_3$ and (c) $BaTiO_3$ in the vicinity of the phase transition. Points are experimental data. Lines are calculated from Eq 6.

Thus, for $HoMnO_3$, an activation process was identified, and activation energy values U_ε were determined near the $T_{SR} \approx 41$ K (Figure 3b). For $BaTiO_3$, the activation energy value U_ε associated with the dielectric permittivity was also determined near the ferroelectric transition at the $T_C \approx 394$ K (Figure 3c). A significant difference in the dielectric permittivity activation energies for these samples should be noted; for $HoMnO_3$ and $BaTiO_3$, this difference reaches three orders of magnitude. This is attributed to the three-order-of-magnitude difference in the ε values. Furthermore, the jump in dielectric permittivity near the transition is more pronounced in $BaTiO_3$. This is due to the significantly weaker excitation of the electronic subsystem in $HoMnO_3$ compared to $BaTiO_3$, resulting in a difference in dielectric permittivity activation energies of more than three orders of

magnitude. In addition, based on experimental data regarding the temperature dependence of the heat capacity of $YMnO_3$, $HoMnO_3$, and $BaTiO_3$, enthalpy values (ΔH) were calculated for the identified processes (Table 2) using the Eq 12:

$$\Delta H = \int \Delta C_p(T) dT \tag{12}$$

Table 2. Calculated enthalpy values from Eq 12 for $YMnO_3$, $HoMnO_3$ and $BaTiO_3$.

Sample	Phase transition	ΔH, J/mol
$YMnO_3$	$T_N \approx 70$ K	62
$HoMnO_3$	$T_N \approx 70$ K	61
$BaTiO_3$	$T_C \approx 394$ K	60

The magnetic orders of $YMnO_3$ and $HoMnO_3$ were determined by the antiferromagnetic in-plane Mn–O–Mn superexchange and were complemented by two orders of magnitude weaker interplane Mn–O–O–Mn exchange in the folded triangular lattice. Eight different magnetic phases of the Mn^{3+} sublattice and at least three different phases of the Y^{3+} and Ho^{3+} sublattices are distinguished. Moreover, magnetic reorientations of the Mn^{3+} lattice can occur through in-phase or out-of-phase rotation of triangularly frustrated spins in adjacent crystallographic planes [45]. For $HoMnO_3$, a noticeable transition is a slight change in the slope of the $\mu(T)$ dependence at 41 K, which is caused by the spin reorientation of the Mn^{3+} sublattice from P6′$_3$c′m to P6′$_3$cm′ (′− corresponds to various possible ordered arrangements of Mn spins in hexagonal rare-earth manganites) [46]. Taking this into account, the value of the activation energy of magnetic permeability U_μ obtained by us in the vicinity of the phase transition at T_{SR} can serve as an estimate parameter of the excitation process of the spin subsystem of $HoMnO_3$, leading to the rotation of triangularly frustrated spins in adjacent crystallographic planes (Figure 4).

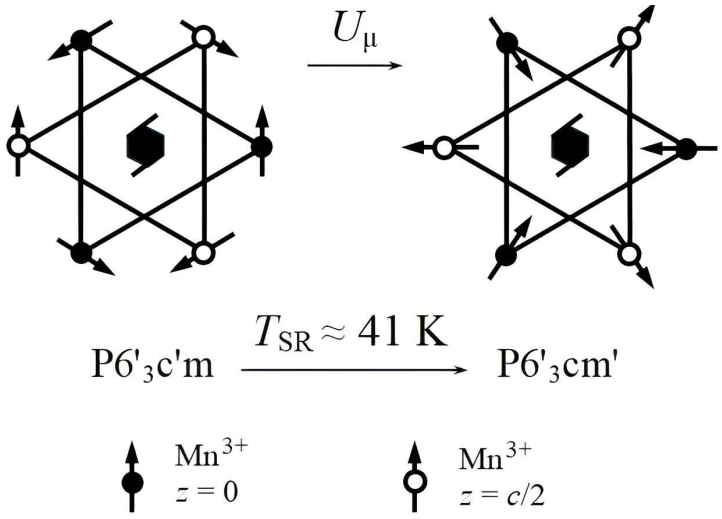


Figure 4. Symmetry change (from P6′$_3$c′m to P6′$_3$cm′) of the antiferromagnetic ordering of $HoMnO_3$ at the $T_{SR} \approx 41$ K. U_μ is the activation energy of magnetic permeability. z and c are the axis and the parameter of the hexagonal crystal lattice, respectively.

In the case of $BaTiO_3$, at temperature T_C, the ferroelectric phase transition occurs as a result of electron-phonon (vibronic) interaction in the presence of electron band mixing and electron orbital degeneracy (or quasi-degeneracy in the case of the pseudo-Jahn-Teller effect) [47]. A decrease in energy with partial or complete removal of electron orbital degeneracy leads to symmetry breaking: a transition from cubic to tetragonal symmetry of the $BaTiO_3$ crystal lattice at temperature T_C with decreasing temperature. In this case, the calculated values of the activation energies of the heat capacity U_C and the permittivity U_ε can serve as an estimate of the excitation process of the electronic subsystem of $BaTiO_3$, leading to electron transitions between the 3*d* and 2*p* levels of titanium and oxygen, respectively, which is accompanied by hybridization of these orbitals (Figure 5).

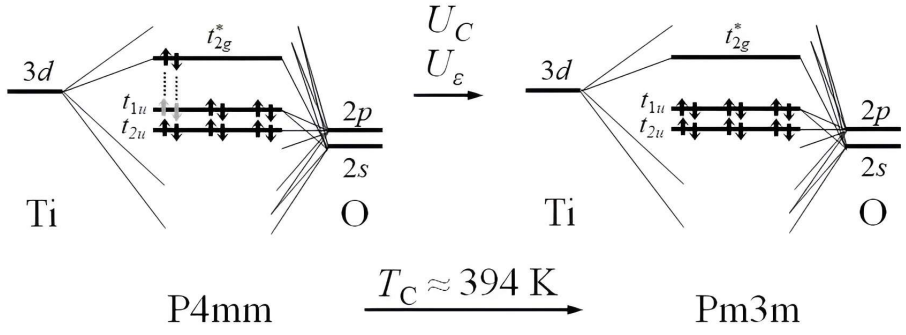


Figure 5. Change in the population of the electron levels of titanium (3*d*) and oxygen (2*p*) in $BaTiO_3$ at the $T_C \approx 394$ K, accompanied by a change in the symmetry of the crystal lattice from tetragonal (P4mm) to cubic (Pm3m). U_C is the activation energy of the heat capacity. U_ε is the activation energy of the permittivity.

It is also worth separately noting the reasons for the differences in the activation energy values in the vicinity of the phase transition for the materials studied. For example, activation energies close to 1 eV, as noted in the introduction, are characteristic of processes caused by the presence of oxygen vacancies in the oxygen-containing materials under consideration.

Higher activation energies (2 eV and higher) may be associated with the presence of electronic transitions between the 3*d* and 2*p* levels of the transition metal and oxygen near the Curie point (due to orbital hybridization and the Jahn-Teller effect). In the case of processes changing the symmetry of the antiferromagnetic ordering at the T_{SR}, activation energies may have even lower values (~10^{-3} eV). Figure 3 shows a difference of 3 orders of magnitude in the permittivity of $HoMnO_3$ and $BaTiO_3$. The jump in permittivity near the phase transition for $BaTiO_3$ is also more significant. This is due to significantly weaker excitation of the electronic subsystem in $HoMnO_3$ compared to $BaTiO_3$, which leads to a difference in the activation energies of the permittivity of more than three orders of magnitude.

4. Conclusions

In this article, we continue our exploration of the possibility of describing the temperature dependences of the electrical, magnetic, and thermal properties of functional materials using an exponential dependence containing the activation energy of the measured physical quantity (magnetic and permittivity, heat capacity), which can be termed “activation analysis”. This method was applied to the ferroelectric $BaTiO_3$ and the antiferromagnetic multiferroics $YMnO_3$ and $HoMnO_3$ to study the

regions near ferroelectric and magnetic phase transitions, which are characterized by significant spin-phonon and electron-phonon interactions. These include:

- A second-order transition from the antiferromagnetic state to the paramagnetic state at the temperature T_N ($YMnO_3$, $HoMnO_3$).
- A first-order magnetostructural transition of the order-to-order type, also known as a spin-reorientation (spontaneous) transition at the temperature T_{SR} ($HoMnO_3$).
- First-order bias-type ferroelectric phase transition ($BaTiO_3$).

Based on the analysis of literary and experimental data, it is assumed that the obtained values of the magnetic permeability activation energy ($U_\mu = 1.53 \times 10^{-5}$ eV) in the vicinity of the phase transition at the T_{SR} temperature can serve as an estimate parameter for the excitation process of the $HoMnO_3$ spin subsystem, leading to the rotation of triangularly frustrated spins in adjacent crystallographic planes. This, through spin and electron-phonon interactions, can lead to the excitation of the electron subsystem with the permittivity activation energy ($U_\varepsilon = 2.77 \times 10^{-3}$ eV).

Additionally, the calculated values of the permittivity activation energy ($U_\varepsilon = 2.28$ eV) can presumably serve as an estimate parameter for the excitation process of the $BaTiO_3$ electron subsystem, leading to electron transitions between the 3*d* and 2*p* levels of titanium and oxygen, respectively, which is accompanied by the hybridization of these orbitals. Due to the significant electron-phonon (vibronic) interaction in the vicinity of the ferroelectric phase transition, the activation energy of the heat capacity ($U_C = 2.29$ eV) is also significant.

The proposed approach to activation analysis of the temperature dependences of the parameters of functional materials in the vicinity of the phase transition enables us to expand the information content of the calculated data, in particular, to determine the excitation energy spectrum of the electron and spin subsystems of ferroelectrics, magnets, and magnetic phonons. This helps us gain new fundamental knowledge about the activation processes of phase transitions in functional materials with significant spin-phonon and electron-phonon coupling.

Use of AI tools declaration

The authors declare they have not used Artificial Intelligence (AI) tools in the creation of this article.

Acknowledgments

The author thanks the staff of the Department of Functional Materials of the Scientific Research Institute “Reaktivelectron” for their assistance in obtaining $BaTiO_3$ ceramic samples for the study.

Author contributions

Danil V. Kuzenko contributed to formulating the research concept and structuring the article, carried out the analysis and synthesis of the literature data, and was responsible for drafting and editing the manuscript. Aleksey V. Bezus provided critical review of the manuscript and approved the final version for publication.

Conflict of interest

The authors declare no conflict of interest. From 2023 to 2025, Danil V. Kuzenko supervised the research project "Activation Mechanisms of Phase Transitions in Ferroelectric Materials," funded by the Ministry of Science and Higher Education of the Russian Federation.

References

1. Weston L, Cui XY, Ringer SP, et al. (2016) Multiferroic crossover in perovskite oxides. *Phys Rev B* 93: 165210. https://doi.org/10.1103/PhysRevB.93.165210
2. Bersuker IB (2012) Pseudo Jahn-Teller origin of perovskite multiferroics, magnetic-ferroelectric crossover, and magnetoelectric effects: The d^0-d^{10} problem. *Phys Rev Lett* 108: 137202. https://doi.org/10.1103/PhysRevLett.108.137202
3. Bansal D, Niedziela JL, Sinclair R, et al. (2018) Momentum-resolved observations of the phonon instability driving geometric improper ferroelectricity in yttrium manganite. *Nat Commun* 9: 15. https://doi.org/10.1038/s41467-017-02309-2
4. Yamauchi K, Picozzi S (2009) Magnetically induced ferroelectricity in $TbMnO_3$: Inverse Goodenough–Kanamori interaction. *J Phys Condens Matter* 21: 064203. https://doi.org/10.1088/0953-8984/21/6/064203
5. Van Aken BB, Palstra TTM, Filippetti A, et al. (2004) The origin of ferroelectricity in magnetoelectric $YMnO_3$. *Nat Mater* 3: 164–170. https://doi.org/10.1038/nmat1080
6. Sakai H, Fujioka J, Fukuda T, et al. (2011) Displacement-type ferroelectricity with off-center magnetic ions in perovskite $Sr_{1-x}Ba_xMnO_3$. *Phys Rev Lett* 107: 137601. https://doi.org/10.1103/PhysRevLett.107.137601
7. Delaire O, Stone MB, Ma J, et al. (2012) Anharmonic phonons and magnons in $BiFeO_3$. *Phys Rev B* 85: 064405. https://doi.org/10.1103/PhysRevB.85.064405
8. Poojitha B, Rubi K, Sarkar S, et al. (2019) Effect of phonon anharmonicity on ferroelectricity in $Eu_xBa_{1-x}TiO_3$. *Phys Rev Mater* 3: 024412. https://doi.org/10.1103/PhysRevMaterials.3.024412
9. Povzner AA, Volkov AG, Nogovitsyna TA (2024) Skyrmions and fluctuations of spin spirals in strongly correlated $Fe_{1-x}Co_xSi$ with a noncentrosymmetric cubic structure. *J Surf Investig* 18: 944–949. https://doi.org/10.1134/S102745102470068X
10. Yakunina EM, Kravtsov EA, Khaydukov YN, et al. (2021) Structure and magnetism in multilayer Fe/MgO/Cr/MgO/Fe nanosystems. *J Surf Investig* 15: 793–798. https://doi.org/10.1134/S1027451021040406
11. Asanov IP, Fedorenko AD, Vasilchenko DB, et al. (2023) Spin-orbit interactions in osmium complexes. *J Surf Investig* 17: 630–640. https://doi.org/10.1134/S1027451023030217
12. Bauer GEW, Tang P, Iguchi R, et al. (2022) Magnonics vs. ferronics. *J Magn Magn Mater* 541: 168468. https://doi.org/10.1016/j.jmmm.2021.168468
13. Zhou XH, Cai C, Tang P, et al. (2023) Surface ferron excitations in ferroelectrics and their directional routing. *Chin Phys Lett* 40: 087103. https://doi.org/10.1088/0256-307X/40/8/087103
14. Wooten BL, Iguchi R, Tang P, et al. (2023) Electric field–dependent phonon spectrum and heat conduction in ferroelectrics. *Sci Adv* 9: eadd7194. https://doi.org/10.1126/sciadv.add7194
15. Nagaev EL (1992) Ferrons and the giant Zeeman effect in amorphous semiconductors. *Phys Solid State* 34: 1882–1888 (in Russian). https://journals.ioffe.ru/articles/22471

16. Vazhenin VA, Rumyantsev E, Artemov MY, et al. (1998) Mechanisms of EPR line broadening in $Pb_5Ge_3O_{11}$ near a structural transition. *Phys Solid State* 40: 293–298. https://doi.org/10.1134/1.1130296
17. Glinchuk MD, Kondakova IV (1998) EPR and NMR line shapes in disordered ferroelectric crystals. *Phys Solid State* 40: 311–317. https://doi.org/10.1134/1.1130300
18. Kallaev SN, Bakmaev AG, Omarov ZM, et al. (2022) Thermophysical properties of multiferroics $Bi_{1-x}Tm_xFeO_3$. *Phys Solid State* 64: 298–301. https://doi.org/10.21883/PSS.2022.02.52979.221
19. Mitarov RG, Kallaev SN, Omarov ZM (2022) Heat capacity of nanostructured $SmFeO_3$. *Phys Solid State* 64: 591–593. https://doi.org/10.21883/PSS.2022.05.53522.272
20. Kallaev SN, Bakmaev AG, Omarov ZM (2023) Thermophysical properties and phase transitions of ferroelectric $PbFe_{0.5}Nb_{0.5}O_3$ at high temperatures. *Phys Solid State* 65: 506–508. https://doi.org/10.21883/PSS.2023.03.55596.562
21. Derets NK, Mikhailin NYu, Smirnova TA, et al. (2024) Study of the temperature behavior of the heat capacity of a relaxor ferroelectric $PbNi_{1/3}Nb_{2/3}O_3$. *Phys Solid State* 66: 1649–1652. https://doi.org/10.61011/PSS.2024.10.59625.222
22. Ovsyannikov GA, Constantinian KY, Ulev GD, et al. (2024) Manganite heterostructures $SrIrO_3/La_{0.7}Sr_{0.3}MnO_3$ and $Pt/La_{0.7}Sr_{0.3}MnO_3$ for generation and registration of spin current. *J Surf Investig* 18: 210–216. https://doi.org/10.1134/S1027451024010336
23. Jankowska-Sumara I, Kądziołka-Gaweł M, Podgórna M, et al. (2020) Complex structure and Mössbauer effect observed in the course of phase transitions in $PbZr_{0.72}Sn_{0.28}O_3$ single crystal. *J Chem Phys* 153: 224202. https://doi.org/10.1063/5.0032957
24. Gokhfeld YS, Kazak NV, Bel'skaya NA, et al. (2023) Structural disorder, specific heat, and magnetic transitions in Cu_2FeBO_5. *J Exp Theor Phys* 137: 494–505. https://doi.org/10.1134/S1063776123100175
25. Shaykhutdinov KA, Skorobogatov S, Knyazev YV, et al. (2024) Controlling the temperature of the spin-reorientation transition in $HoFe_{1-x}Mn_xO_3$ orthoferrite single crystals. *J Exp Theor Phys* 165: 693–706. https://doi.org/10.31857/S004445102405e080
26. Googlev KA, Kozakov AT, Kochur AG, et al. (2025) Crystal and electronic structure of the composite compound $Bi_{1-x}La_xFe_{1-y}Mn_yO_{3+\sigma}$ according to *X*-ray diffraction and *X*-ray electron spectroscopy. *Phys Solid State* 67: 285–290. https://doi.org/10.61011/PSS.2025.02.60679.348
27. Khan AR, Bhardwaj S, Kumar S (2025) Influence of Fe^{3+} and Co^{2+} co-doping on the electrical, magnetodielectric, and multiferroic properties of lead-free $Ba_{0.7}Sr_{0.3}TiO_3$ ceramics. *J Magn Magn Mater* 624: 173030. https://doi.org/10.1016/j.jmmm.2025.173030
28. Motseyko AV, Pushkarev AV, Olekhnovich NM, et al. (2025) Magnetic phase transitions in $(1-x)BiFeO_3–xPbFe_{1/2}Sb_{1/2}O_3$ solid solutions studied by the Monte Carlo method. *Comput Mater Sci* 253: 113860. https://doi.org/10.1016/j.commatsci.2025.113860
29. Evarestov RA, Novikov SS (2025) Non-empirical calculations of properties of $KNbO_3$ and $RbNbO_3$ crystals. *Phys Solid State* 67: 259–267. https://doi.org/10.61011/PSS.2025.02.60674.32-25
30. Picozzi S, Yamauchi K, Sergienko IA, et al. (2008) Microscopic mechanisms for improper ferroelectricity in multiferroic perovskites: A theoretical review. *J Phys Condens Matter* 20: 434208. https://doi.org/10.1088/0953-8984/20/43/434208

31. Zhukov VP, Chulkov EV (2022) Electronic band structure and thermoelectric properties of $SrTiO_3$, $BaTiO_3$ and $CaTiO_3$: ab initio approach. *Phys Solid State* 64: 1855–1863. https://doi.org/10.21883/PSS.2022.12.54377.383
32. Tomczyk M, Vilarinho PM, Moreira A, et al. (2011) High temperature dielectric properties of $YMnO_3$ ceramics. *J Appl Phys* 110: 064116. https://doi.org/10.1063/1.3629996
33. Warren WL, Vanheusden K, Dimos D, et al. (1996) Oxygen vacancy motion in perovskite oxides. *J Am Ceram Soc* 79: 536–538. https://doi.org/10.1111/J.1151-2916.1996.TB08162.X
34. Sundarakannan B, Kakimoto K, Ohsato H (2003) Frequency and temperature dependent dielectric and conductivity behavior of $KNbO_3$ ceramics. *J Appl Phys* 94: 5182–5187. https://doi.org/10.1063/1.1610260
35. Kuzenko DV (2024) Activation analysis of the temperature dependence of the dielectric constant of ferroelectrics. *Bull Russ Acad Sci Phys* 88: 715–720. https://doi.org/10.1134/S1062873824706470
36. Fan C, Zhao ZY, Song JD, et al. (2014) Single crystal growth of the hexagonal manganites RMnO$_3$ (R = rare earth) by the optical floating-zone method. *J Cryst Growth* 388: 54–60. https://doi.org/10.1016/j.jcrysgro.2013.11.028
37. Kuzenko DV (2021) Critical temperature below the Curie temperature of ferroelectric ceramics PZT. *J Adv Dielectr* 11: 2150006. https://doi.org/10.1142/S2010135X21500065
38. Kuzenko DV (2024) Determination of the activation energy of defects in ferroelectrics by the method of temperature activation–relaxation of the dielectric permittivity. *J Surf Investig* 18: 530–535. https://doi.org/10.1134/S1027451024700058
39. Belov KP, Zvezdin AK, Kadomtseva AM, et al. (1976) Spin-reorientation transitions in rare-earth magnets. *Sov Phys Usp* 19: 574–596. https://doi.org/10.1070/PU1976v019n07ABEH005274
40. Bussmann A, Bilz H, Roenspiess R, et al. (1980) Oxygen. polarizability in ferroelectric phase transitions. *Ferroelectrics* 25: 343–346. https://doi.org/10.1080/00150198008207016
41. Kuzenko DV (2025) Construction of the interatomic potential of the ferroelectric barium titanate based on the temperature dependence of the heat capacity near the phase transition. *Phys Solid State* 67: 502–509. https://doi.org/10.61011/PSS.2025.03.60881.54-25
42. Smolensky GA (1985) *The Physics of Ferroelectric Phenomena*, Leningrad: Izdatel'stvo Nauka (in Russian).
43. Mushnikov NV (2017) *Magnetism and Magnetic Phase Transitions*, Ekaterinburg: Publishing house of the Ural. University (in Russian).
44. Murtazaev AK, Abdulvagidov SB, Aliev AM, et al. (2001) Heat capacity of a Cr_2O_3 antiferromagnet near the critical temperature. *Phys Solid State* 43: 1103–1107. https://doi.org/10.1134/1.1378152
45. Brown PJ, Chatterji T (2006) Neutron diffraction and polarimetric study of the magnetic and crystal structures of $HoMnO_3$ and $YMnO_3$. *J Phys Condens Matter* 18: 10085–10096. https://doi.org/10.1088/0953-8984/18/44/008
46. Fiebig M, Lottermoser Th, Pisarev RV (2003) Spin-rotation phenomena and magnetic phase diagrams of hexagonal RMnO$_3$. *J Appl Phys* 93: 8194–8196. https://doi.org/10.1063/1.1544513

47. Bersuker IB (2001) Vibronic (pseudo Jahn-Teller) theory of ferroelectricity: Novel aspects and applications. *Ferroelectrics* 536: 1–59. https://doi.org/10.1080/00150193.2018.1528919



AIMS Press

© 2026 the Author(s), licensee AIMS Press. This is an open access article distributed under the terms of the Creative Commons Attribution License (http://creativecommons.org/licenses/by/4.0)